DOI: 10.1002/ ((please add manuscript number))
Article type: Full Paper

Highly Sensitive Detection of Polarized Light Using Anisotropic Two-Dimensional ReS_2

Fucai Liu[†]*, Shoujun Zheng*[†]*, Xuexia He*[*]*, Apoorva Chaturvedi, Junfeng He, Wai Leong Chow, Thomas R. Mion, Xingli Wang, Jiadong Zhou, Qundong Fu, Hong Jin Fan, Beng Kang Tay, Li Song, Rui-Hua He, Christian Kloc, Pulickel M. Ajayan, Zheng Liu*[*]

Dr. Fucai Liu, Dr. Xuexia He, Apoorva Chaturvedi, Jiadong Zhou, Qundong Fu, Prof. Christian Kloc, Dr. Zheng Liu
School of Materials Science and Engineering, Nanyang Technological University, Singapore 639798, Singapore.
E-mail: z.liu@ntu.edu.sg, xxhe@ntu.edu.sg,
Shoujun Zheng, Dr. Hong Jin Fan
Centre for Disruptive Photonic Technologies, School of Physics and Mathematics Sciences, Nanyang Technological University, Singapore 637371, Singapore
Wai Leong Chow, Xingli Wang, Prof. Dr. Beng Kang Tay
School of Electrical and Electronic Engineering, Nanyang Technological University, Singapore 639798, Singapore.
Dr. Junfeng He, Thomas R. Mion, Dr. Rui-Hua He
Department of Physics, Boston College, Chestnut Hill, Massachusetts 02467, USA
Wai Leong Chow, Prof. Beng Kang Tay, Dr. Zheng Liu
CINTRA CNRS/NTU/THALES, UMI 3288, Research Techno Plaza, 50 Nanyang Drive, Border X Block, Level 6, Singapore 637553, Singapore.
Prof. Li Song
National Synchrotron Radiation Laboratory, University of Science and Technology of China, Hefei, Anhui 230026, P.R. China
Prof. Pulickel M. Ajayan
Department of Materials Science and Nanoengineering, Rice University, Houston, Texas 77005, USA.
†Fucai Liu and Shoujun Zheng contributed equally to this work.

Keywords: ReS_2, 2D materials, Anisotropy, Photoresponse, Linear dichroism

Abstract: Due to the novel optical and optoelectronic properties, two dimensional (2D) materials have received increasing interests for optoelectronics applications. Discovering new properties and functionalities of 2D materials are challenging yet promising. Here broadband polarization sensitive photodetectors based on few layer ReS_2 are demonstrated. The transistor based on few layer ReS_2 shows an n-type behavior with the mobility of about 40 $cm^2V^{-1}s^{-1}$ and on/off ratio of 10^5. The polarization dependence of photoresponse is ascribed to the unique anisotropic in-plane crystal structure, consistent with the optical absorption anisotropy. The linear dichroic photodetection with a high photoresponsivity reported here demonstrates a route to exploit the intrinsic anisotropy of 2D materials and the possibility to open up new ways for the applications of 2D materials for light polarization detection.

1. Introduction

Light polarization is an important concept in optics, discussing the generation, detection and manipulation of light with certain vibration direction and period. Detection of light polarization has been adapted to various fields, ranging from communication, near field imaging, remote sensing, as well as to military applications[1]. It demands the capability of high detection sensitivity yet compactness for achieving a high level of integration and flexibility. By far, devices commercially available are incapable of meeting these requirements. Most technological implementations integrate the detection component with polarization element in a non-monolithic platform. In addition, a flexibly integrated device will enable a better adaptability of the polarized optical system, while classic quantum-well based photodetectors, which utilizes a grating to couple the incident light into the quantum wells, are not suitable to flexible applications[2]. In order to examine the direction of polarization in an efficient and convenient way, certain materials like nanowire or carbon nanotube have been proposed because of their intrinsically high sensitivity and flexibility[3,4]. However, these materials require sophisticated technologies to pattern the devices and align channel materials. The emerging 2D materials such as graphene and MoS_2 shed a light to the detection of polarization due to their unique crystal structures and high sensitivity to the light.

When materials are scaled to two dimensional, or even to monolayer limit, they exhibit unique properties and phenomena which are distinct from their bulk counterparts. This emerges primarily due to the quantum confinement effect[5-9]. For example, room temperature quantum Hall effect has been observed in graphene[10-12]. From the aspect of optical behaviors, an indirect to direct band crossover, valley-selective circular dichroism, and large exciton binding energy showed up in transition metal dichalcogenides (TMDs) like MoS_2 and WS_2[13-17]. Though a very promising candidate, there are few reports on the detection of polarized light using 2D materials[18-20]. ReS_2 is a typical layered TMD with a band gap of 1.5 eV. It has distorted 1T highly-anisotropic in-plane structure which will induce electrons and photons with anisotropic nature within the layer plane [21,22]. In addition, ReS_2 has been reported to have vanishing interlayer coupling[23], and integrated inverter based on the conductivity anisotropy of ReS_2 has been demonstrated[24]. ReS_2 has also been used as a platform for the study of ballistic transport[25]. These unique properties of ReS_2 may enable a new research field of electronics and photonics device where the strong anisotropic properties of 2D materials can be used to design conceptually novel electronic and optoelectronic device applications. In this article, a polarization sensitive photodetector with high photoresponsivity is demonstrated based on atomically thin ReS_2, benefiting from the anisotropic nature of the material itself. It is completely different from existing photodetectors for polarization sensitive detection which requires the use of extra components such as gratings to couple the incident light[26]. Our study shows that atomically thin ReS_2 may pave a promising way to the applications on the integrated photonic circuits, optical switches and interconnects for detecting the various orientations of linearly polarized light in a highly integrated photonic platform.

2. Characterization of ReS_2 flakes

Similar to the layered structure of other TMDs, ReS_2 crystalizes in a lattice with strong covalent in-plane bonds and weak van der Waals inter-layer interactions (**Figure 1**a, side view of ReS_2). Such strong anisotropy from the asymmetric structure bonds leads to many anisotropic behaviors, such as their electrical and optical property difference between the directions parallel and perpendicular to the layers. Besides, the distorted $CdCl_2$ layer structure of ReS_2 leads to triclinic symmetry and large in-plane anisotropy[27], which is significantly different from other TMDs with hexagonal structures like MoS_2. Figure 1b shows the top view of ReS_2 crystal structure. We can see that Peierls distortion of the 1T structure results in buckled S layers and zigzag Re chains along one of the lattice vectors (*b*-axis) in the plane. The intrinsic anisotropy of ReS_2 provides a new degree of freedom to manipulate its optical and optoelectronic properties for novel integrated device applications.

To investigate the optical and electrical properties of the ReS_2 atomically thin flakes, a scotch tape based mechanical exfoliation method was used to peel thin flakes from bulk crystal onto degenerately doped silicon wafer covered with 285 nm SiO_2[28]. The morphology and thickness of the exfoliated ReS_2 were characterized by optical microscopy, High Resolution Transmission Electron Microscopy (HRTEM) and Atomic Force Microscopy (AFM), respectively. Figure 1c and d shows the HRTEM images and corresponding Fast Fourier Transform (FFT) pattern taken from few layer ReS_2 flake, confirming high crystallinity of the exfoliated ReS_2. The distortion of Re atom arrangement from perfect hexagonal symmetry creates a distortion of the S atom arrangement in the layer plane. The Re chained formed by distortion is clearly seen in the TEM image aloght the b-axis. The structural anisotropy leads to orientation-dependent electric and optical properties, which will discussed in details below. **Figure 2**a shows the typical optical image of ReS_2 thin flake on SiO_2 substrate. The AFM image of the ReS_2 flake is shown in Figure 2b. The monolayer ReS_2 can be identified from the line profile displayed in Figure 2c. Figure 2d shows the Raman spectrum for ReS_2 of monolayer, few layer (3 nm) and bulk, respectively. The observed 15 vibrational modes in the 100-400 cm^{-1} range are associated with fundamental Raman modes (A_{1g}, E_{2g}, and E_{1g}) coupled to each other and to acoustic phonons, which is significantly different from TMDs with higher hexagonal symmetries[30,31], indicating the structure anisotropy of ReS_2. The main peaks at 150 cm^{-1} and 210.5 cm^{-1} are corresponding to the in-plane (E_{2g}) and mostly out-of-plane (A_{1g}-like) vibration modes, respectively. The peak positions are slightly different from the reported one, which is due to the differences of excitation laser wavelengths of 488 nm in the literature and 532 nm in this study[32]. When the thickness is thinned down to monolayer, the main Raman peaks show very small change due to weak interlayer coupling in ReS_2, which is consistent with previous report[23].

In TMDs with perfect in-plane hexagonal lattice, different M points in the Brillouin zone (eg. M1 and M2 in **Figure 3**a) are equivalent due to the 6-fold symmetry. Therefore, the electronic dispersion along Γ-M1 and Γ -M2 should be identical. However, this case changes when lattice distortion takes place in ReS_2, which breaks the original symmetry and makes M1 and M2 inequivalent. Angle-resolved photoemission spectroscopy (ARPES) measurements have been carried out to study the electronic band dispersion along Γ-M1 and Γ -M2, respectively. Energy distribution curves (EDC) 2nd derivative images have been used to enhance the electronic structures and plotted in Figures 3a and 3c with their momentum locations shown in Figure 3a. Clear differences can be recognized between the dispersion along Γ-M1 and Γ -M2, consistent with the theoretical calculations[23].

The structure anisotropy is always associated with the optical and electrical property anisotropies. In order to examine the in-plane optical anisotropy, we measured the polarization dependence of the absorption spectrum for cleaved ReS_2 thin fake on a quartz substrate using the microscopic spectrophotometer. Inset of **Figure 4**a shows the optical image and orientation indication of crystal used for the measurement. Large anisotropy of absorption is observed by changing the polarization angle from 0^0 to 90^0 (with respect to the *b*-axis). Surprisingly the anisotropy is observed in a wide range from 1.55 eV (800 nm) to 2.76 eV (450 nm) (Figure 4a), which is different from previous reports in bulk samples, in which anisotropy is only observed in a small range around the band edge[33,34], this probably originates from the enhanced transmission of light for the ultrathin ReS_2 layer. The broadband anisotropic absorption re-ignites interests for the study of polarization sensitive photodetector used in the visible to near infrared spectrum. Figure 4b plotted the absorption as a function of the polarization angle. The curve can be fitted with a sinusoidal function, which is identical to the band-edge absorption and Raman spectra spectrum change in anisotropic materials[33,35]. This in-plane anisotropy of ReS_2 is attributed to the field-induced polarization of the lattice, which leads to displacements of the lattice atoms, and consequently affects the electronic states of the solids[36]. The peak observed near band edge is related to the exciton absorption[37], which is also polarization dependent, shifting from 1.51 eV to 1.48 eV by rotating the polarization from perpendicular to parallel *b*-axis direction (see the inset in Figure 4a). This polarization dependence of exciton absorption can be used for the wavelength and polarization sensitive luminescent applications.

3. Electronic transport and photoresonse properties of ReS_2 transistor

Electronic properties have a pronounced effect on the performance of photodetection. Before examining the photodetector performance, we first fabricated the field effect transistors (FETs) using atomically thin ReS_2 and studied their transport performances. The transistor was fabricated using the photolithography, following the deposition of Cr/Au (5/50 nm) electrode using the high vacuum thermal evaporator. In order to study the polarization dependence of ReS_2 FET later, the conduction channels were made along the *b*-axis direction. **Figure 5**a shows the output characteristics of the device based on the flake with a thickness of about 3 nm, indicating an obvious n-type semiconducting behavior of ReS_2. The linear I_d-V_d curve under low drain voltage indicates negligible Schottky barrier at the ReS_2 and Cr/Au interfaces. When the gate voltage was varied from -30 V to 30 V while applying 0.1 V drain voltage, as shown in Figure 5b, the channel switched from off state to on state and an increase in drain current by a factor of 10^5 was observed. The measured on/off ratio is four orders of magnitude larger than those in graphene and comparable to the value recently reported in

MoS_2 device[38]. The field-effect mobility was estimated from the linear region in the I_d-V_g curve (Vg from 10 V to 30 V) by using the equation $\mu = \frac{dI_d}{dV_g} \times \frac{L}{WC_iV_d}$, where L is the channel length, W is the channel width and C_i is the capacitance between the channel and the back gate per unit area ($C_i = \varepsilon_0 \varepsilon_r / d$; ε_0 is the vacuum permittivity, ε_r is the relative permittivity, and d is the thickness of SiO_2 layer), respectively. The mobility is calculated to be around 18 $cm^2V^{-1}s^{-1}$, with L = 6.2 μm, W = 1.7 μm, and d = 285 nm. This value is comparable to the values from exfoliated MoS_2 layers. Further improvement of the mobility will be achieved by optimizing the contact metals, the interface between the channel and gate dielectric or using high-k gate dielectric screening[38-40].

To understand the mechanisms of limiting the mobility in ReS_2, we examined the temperature dependence of the mobility from room temperature to 100 K (Figure 5c and 5d). By decreasing the temperature, the mobility increased monotonically to 40 $cm^2V^{-1}s^{-1}$, due to the weak electron-phonon scattering at low temperature[41]. As shown in the inset of Figure 5d, the temperature dependence can be fitted by the power law $\mu \propto T^{-\gamma}$, where the exponent γ is about 1.1, which depends on the dominant phonon scattering mechanism. This value is same as that reported for bilayer MoS_2[42], and is smaller than that of monolayer MoS_2 and theoretical calculation[41, 43]. Although some variations in the apparent phonon damping factor may be explained by charged impurity scattering and homopolar phonon quenching[42], the origin of the observed γ in our work is still unclear, more experimental and theoretical calculation, including much lower temperature measurement combining with the Hall mobility measurement, will be of much help for fully understanding the scattering mechanism and optimizing the device performance for ReS_2 and other 2D materials.

The good electronic properties of ReS_2 make it promising for the application of optoelectronic devices. In addition, the direct band gap nature of this material results in both a high absorption coefficient and efficient electron-hole pair generation under photoexcitation, which is crucial for high-performance photodetectors. We examined the photoresponse properties of atomically thin ReS_2 (~3 nm) in the two-terminal device geometry, using a typical green semiconductor laser (2.4 eV) as the illumination source (**Figure 6**a). The photoresponse under different wavelength excitations is also investigated and shown in Figure S1. The device shows good response to all the wavelength lights. Figure 6b shows the photocurrent as a function of drain bias. By increasing the light power the photocurrent becomes stronger. In Figure 6c, we have extracted the light power dependence of photocurrent at different drain voltages. It can clearly be seen that the photocurrent satisfies a simple power law relation $I_{ph} \propto p^{\alpha}$, where I_{ph} is the photocurrent, P is the light power, respectively. The index of power law α is deduced to be 0.3, which is attributed to complex processes in the carrier generation, trapping, and electron-hole recombination in the semiconductor[44]. The process for the photocurrent generation can be explained by a simplified energy band diagram (Figure 6d). The charge transfer via Femi level tuning between the interface of metal electrodes and ReS_2 channels, resulting in the band bending, and therefore forming Schottky type barriers as well as a depletion layers. Under the light illumination with the photon energy greater than the energy gap of the semiconductor, electron-hole pairs are excited by absorbing light and laterally separated by the applied drain bias, leading to the generation of photocurrent. The response of photodetector is proportional to the rate of incident beams of photons, which is consistent with the result in Figure 6c. The time dependent photoresponse of the ReS_2 device carried out by mechanically modulating the intensity of the incoming light and recording the current change, and shown in Figure S2. Photoresponsivity R, as the ratio between the intensity of generated photocurrent to that of the incident light, is one of the most important parameters for a photodetector. Figure 6e shows the photoresponsivity evaluated at different bias voltages from Figure 6b, respectively. The device achieved a photoresponsivity of 10^3

AW^{-1} at low intensity of light. This value is several orders of magnitude higher than that of graphene-based photodetectors[45]. It is also comparable with the highest value of MoS_2-based photodetectors[46], and is three orders of magnitude higher than that of black phosphorus[47]. A sub-linear dependence of the photoresponse was observed upon tuning the light power. The presence of the trap states either in the channel or at the interface between ReS_2 and the underlying SiO_2 layer may be responsible for the reduction of the photoresponsivity at higher light power[46].

The structure anisotropy induced linear dichroism in ReS_2 enables us to study the polarization sensitive photodetector. We now focus our study on the polarization sensitive detection of the device. The polarization of the illuminated light is controlled via the combination of one half wave plate and a polarizer. Figure 7a shows the evolution of photocurrent as a function of the polarization angle of the linear polarizer. By rotating the polarization of the light while keeping the incident power constant, the photocurrent changes dramatically. The photocurrent with the incident light polarized along the *b*-axis (defined as 90º see inset of Figure 4a) is much stronger than that perpendicular to the *b*-axis (defined as 0º). This is a strong evidence that demonstrates the polarization dependent absorption and resulting photocurrent detection via linear dichroism. The photocurrents under drain voltages of 1 V, 2 V and 3 V as a function of incident light polarization angle are shown in Figure 7b. The data can be perfectly fitted by a sinusoidal function. In addition, the photocurrent and absorption has a quite similar dependence on the incident light polarization, as shown in Figure 7c, which are plotted in the same polar coordination. This strongly suggests that the intrinsic polarization dependent photoresponse originates from ReS_2 itself. These observations clearly indicate that the incident light in different polarization states passing through the anisotropic ReS_2 experiences a varying absorption, directly reflecting the intrinsically anisotropic nature of the crystal structure. Due to the varying absorption in the wide wavelength range seen from the absorption spectrum, the polarization sensitive photodetection can be extended to a wide range from visible to near infrared. Compared to the reported polarization sensitive device based on a wire-grid polarizer relying on nanofabrication processes[26], our demonstrations prove that atomically thin ReS_2 can be used as a potential intrinsic linear dichroism media with high responsivity for practical integrated optical applications.

4. Conclusion

In this work, we have studied the electronic and photoresponse properties of atomically thin ReS_2 obtained by mechanical exfoliation method. The electron mobility up to 40 $cm^2V^{-1}s^{-1}$ was obtained with an on/off ratio of about 10^5. The device also shows a good photoresponse with a photoresponsivity of 10^3 A W^{-1}. The linear dichroic photodetector based on anisotropic ReS_2 is demonstrated, which is ascribed to the polarization sensitive absorption induced by crystal structure anisotropy. Combining with the environmental stability and unique physical properties like weak interlayer coupling of ReS_2, together with the high flexibility of 2D materials[48], the linear dichroism observed in ReS_2 leads to a new degree of freedom to manipulate electronic and optoelectronic properties and opens up exciting opportunities of novel integrated optical and optoelectronic device applications for polarization detection. The advantage of the simple transistor architecture reported here allows the polarization dependent phototransistor to be used as part of a circuit, for example, as part of a complementary inverter or ring oscillator. Recent progress in growth of 2D materials and heterostructure[49-51], should allow the creation of arrays of micrometre-scale devices, as well as integration with CMOS electronics and ultimate thin single-layer light polarization detection devices based on anisotropic ReS_2 and other 2D materials[46, 52].

5. Experimental Section

Isolation and characterization of ReS_2 flake. The ReS_2 single crystals were synthesized through chemical vapor transport using iodine as the transport agent. A scotch-tape method was used to exfoliate ReS_2 flakes on the degenerately doped Si substrate covered with 285 nm

SiO_2. Optical identification was conducted with Olympus BX51 microscope. Thickness of the thin flake was measured by Asylum Research Cypher S Atomic Force Microscopy (AFM) in trapping mode. Raman spectrum characterization was performed using Witec confocal Raman system under 532 nm laser excitation. HRTEM image was obtained using FEI Tecnai F20 system. The ARPES experiments were carried out at Beamline 5-4 of the Stanford Synchrotron Radiation Lightsourse (SSRL) of Slac National Accelerator Laboratory using 25 eV photons with a base pressure better than 5×10^{-11} Torr. Absorption spectrum was characterized by Jasco MSV-5200 microscopic spectrophotometer.

Device fabrication and measurement. The electrodes were patterned via photolithography, followed by thermal evaporation of Cr/Au (5/50 nm) and subsequent lift-off process. Electric characterization was performed by using the Aglient B1500 semiconductor parameter analyzer. Low temperature measurement was performed in a probe station cooled by liquid nitrogen. The photoresponse was measured using a semiconductor green laser as the illumination source, in the ambient ocndition. Light power dependence of the photoresponse was performed by tuning the light power while keeping the light polarization unchanged. Polarization dependence of the photoresponse was carried out by rotating the polarization of the light using a half wave plate and a polarizer, while keeping the light power unchanged throughout the measurement.

Supporting Information

Supporting Information is available from the Wiley Online Library or from the author.

Acknowledgements

F.L. and S.Z. contributed equally to this work. The authors acknowledge Zhen Fei and Chuanhong Jin from the Center for Electron Microscopy Zhejiang University China for the help on the HRTEM characterization. This work is supported by the Singapore National

Research Foundation under NRF RF Award No. NRF-RF2013-08, the start-up funding from Nanyang Technological University (M4081137.070). H.J.F. thanks the support from the Ministry of Education of Singapore (Grant No. MOE2011-T3-1-005). T.R.M. acknowledges the support by NSF Fellowship (NSF GRFP DGE-1258923).

Received: ((will be filled in by the editorial staff))
Revised: ((will be filled in by the editorial staff))
Published online: ((will be filled in by the editorial staff))

[1] J. S. Tyo, D. L. Goldstein, D. B. Chenault, J. A. Shaw, *Appl. Opt.* **2006,** *45*, 5453-5469.

[2] C. Chen, K. Choi, L. Rokhinson, W. Chang, D. Tsui, *Appl. Phys. Lett.* **1999,** *74,* 862-864.

[3] J. Wang, M. S. Gudiksen, X. Duan, Y. Cui, C. M. Lieber, *Science* **2001**, *293,* 1455-1457.

[4] X. He, X. Wang, S. Nanot, K. Cong, Q. Jiang, A. A. Kane, J. E. Goldsmith, R. H. Hauge, F. Léonard and J. Kono, *ACS nano* **2013**, *7*, 7271-7277.

[5] Q. H. Wang, K. Kalantar-Zadeh, A. Kis, J. N. Coleman, M. S. Strano, Electronics and optoelectronics of two-dimensional transition metal dichalcogenides. *Nat. Nanotechnol.* **2012,** *7*, 699-712.

[6] F. Koppens, T. Mueller, P. Avouris, A. Ferrari, M. Vitiello, M. Polini, *Nat. Nanotechnol.* **2014**, *9*, 780-793.

[7] M. Chhowalla, H. S. Shin, G. Eda, L.-J. Li, K. P. Loh, H. Zhang, *Nat. Chem.* **2013**, *5,* 263-275.

[8] G. Fiori, F. Bonaccorso, G. Iannaccone, T. Palacios, D. Neumaier, A. Seabaugh, S. K. Banerjee, L. Colombo, *Nat. Nanotechnol.* **2014**, *9*, 768-779.

[9] F. Xia, H. Wang, D. Xiao, M. Dubey, A. Ramasubramaniam, *Nat. Photonics* **2014**, *8*, 899-907.

[10] K. Novoselov, A. K. Geim, S. Morozov, D. Jiang, M. K. I. Grigorieva, S. Dubonos, A. Firsov, *Nature* **2005**, *438*, 197-200.

[11] K. S. Novoselov, Z. Jiang, Y. Zhang, S. Morozov, H. Stormer, U. Zeitler, J. Maan, G. Boebinger, P. Kim, A. Geim, *Science* **2007**, *315*, 1379-1379.

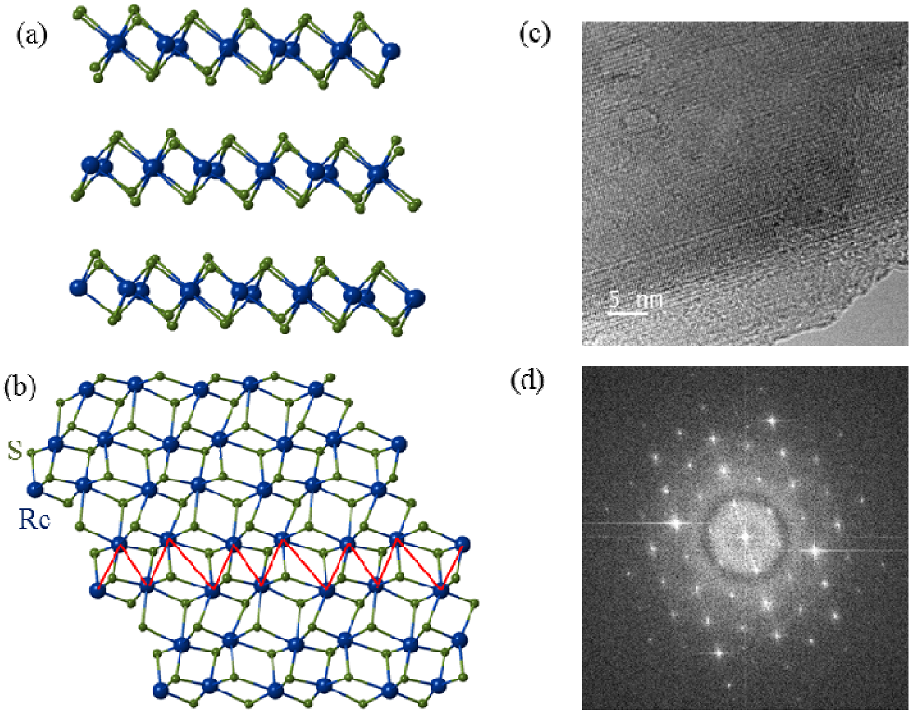

[12] Y. Zhang, Y.-W. Tan, H. L. Stormer, P. Kim, Experimental observation of the quantum Hall effect and Berry's phase in graphene. *Nature* **2005**, *438*, 201-204.

[13] A. Chernikov, T. C. Berkelbach, H. M. Hill, A. Rigosi, Y. Li, O. B. Aslan, D. R. Reichman, M. S. Hybertsen, T. F. Heinz, *Phys. Rev. Lett*. **2014**, *113*, 076802.

[14] K. F. Mak, K. He, J. Shan, T. F. Heinz, *Nat. Nanotechnol*. **2012**, *7*, 494-498.

[15] K. F. Mak, C. Lee, J. Hone, J. Shan, T. F. Heinz, *Phys. Rev. Lett.* **2010**, *105*, 136805.

[16] H. Zeng, J. Dai, W. Yao, D. Xiao, X. Cui, *Nat. Nanotechnol.* **2012**, *7*, 490-493.

[17] Z. Ye, T. Cao, K. O'Brien, H. Zhu, X. Yin, Y. Wang, S. G. Louie, X. Zhang, *Nature* **2014**, *513*, 214-218.

[18] T. Hong, B. Chamlagain, W. Lin, H.-J. Chuang, M. Pan, Z. Zhou and Y.-Q. Xu, *Nanoscale* **2014**, *6*, 8978-8983.

[19] F. N. Xia, H. Wang, Y. C. Jia, *Nat. Commun.* **2014**, *5*, 4458.

[20] H. Yuan, X. Liu F. Farzaneh Afshinmanesh, W. Li, G. Xu, J. Sun, B. Lian, A. G. Curto, G. Ye,Y. Hikita, Z. Shen, S.-C. Zhang, X. Chen, M. Brongersma, H. Y. Hwang, Y. Cui, *Nat. Nanotechnol.* **2015***,* doi:10.1038/nnano.2015.112 .

[21] J. Wilson, A. Yoffe, *Adv. Phys.* **1969**, *18*, 193-335.

[22] Y. Feng, W. Zhou, Y. Wang, J. Zhou, E. Liu, Y. Fu, Z. Ni, X. Wu, H. Yuan, F. Miao, B. Wang, X. Wan, D. Xing, arXiv:1502.02835 **2015**.

[23] S. Tongay, H. Sahin, C. Ko, A. Luce, W. Fan, K. Liu, J. Zhou, Y.-S. Huang, C.-H. Ho, J. Yan, D. F. Ogletree, S. Aloni, J. Ji, S. Li, J. Li, F. M. Peeters, J. Wu, *Nat. commun.* **2014,** *5,* 3252 (2014).

[24] E. Liu*,* Y. Fu, Y. Wang, Y. Feng, H. Liu, X. Wan, W. Zhou, B. Wang, L. Shao, C.-H. Ho, Y.-S. Huang, Z. Cao, L. Wang, A. Li, J. Zeng, F. Song, X. Wang, Y. Shi, H. Yuan, H. Y. Hwang, Y. Cui, F. Miao, D. Xing, *Nat. commun.* **2014***,* *6*, 6991.

[25] Q. Cui, H. Zhao. *ACS nano* **2015**, *9*, 3935-3941.

[26] S. Ura, H. Sunagawa, T. Suhara, H. Nishihara. Focusing grating couplers for polarization detection. *J Lightwave Technol.* **1988**, *6*, 1028-1033.

[27] H. Murray, S. Kelty, R. Chianelli, C. Day. *Inorg. Chem.* **1994**, *33*, 4418-4420.

[29] K. Novoselov, D. Jiang, F. Schedin, T. Booth, V. Khotkevich, S. Morozov, A. Geim, Two-dimensional atomic crystals. *Proc. Natl. Acad. Sci. USA* **2005**, *102*, 10451-10453.

[30] A. Berkdemir, H. R. Gutierrez, A. R. Botello-Mendez, N. Perea-Lopez, A. L. Elias, C.-I. Chia, B. Wang, V. H. Crespi, F. Lopez-Urisa, J.-C. Charlier, H. Torrones, M. Terrones, *Sci. Rep.* **2013**, *3*, 1755.

[31] H. Li*,* Q. Zhang, C. C. R. Yap, B. K. Tay, T. H. Tong, A. Olivier, D. Baillargeat, *Adv. Funct. Mater.* **2012**, *22*, 1385-1390.

[32] T. Fujita, Y. Ito, Y. Tan, H. Yamaguchi, D. Hojo, A. Hirata, D. Voiry, M. Chhowalla, M. Chen, *Nanoscale* **2014**, *6*, 12458-12462.

[33] C. Ho, Y. Huang, K. Tiong, P. Liao. *J Phys. Condens. Matter.* **1999**, *11*, 5367.

[34] G. Dresselhaus, *Phys. Rev.* **1957**, *105*, 135-138.

[35] S. Zhang,J. Yang, R. Xu, F. Wang, W. Li, M. Ghufran, Y.-W. Zhang, Z. Yu, G. Zhang, Q. Qin, Y. Lu, *ACS Nano* **2014**, *8*, 9590-9596.

[36] G. Weiser. *Surf. Sci.* **1973**, *37*, 175-197.

[37] C. Ho, P. Liao, Y. Huang, K. Tiong. *Phys. Rev. B* **1997**, *55*, 15608-15613.

[38] B. Radisavljevic, A. Radenovic, J. Brivio, V. Giacometti, A. Kis. *Nat. Nanotechnol.* **2011**, *6*, 147-150.

[39] W. Liu, J. Kang, D. Sarkar, Y. Khatami, D. Jena, K. Banerjee. *Nano Lett.* **2013**, *13*, 1983-1990.

[40] B. Chamlagain, Q. Li, N. J. Ghimire, H.-J. Chuang, M. M. Perera, H. Tu, Y. Xu, M. Pan, D. Xiao, J. Yan, *ACS Nano* **2014,** *8*, 5079-5088.

[41] B. Radisavljevic, A. Kis, *Nat. Mater.* **2013**, *12*, 815-820.

[42] B. W. Baugher, H. O. Churchill, Y. Yang, P. Jarillo-Herrero. *Nano Lett.* **2013**, *13*, 4212-4216.

[43] K. Kaasbjerg, K. S. Thygesen, K. W. Jacobsen. *Phys. Rev. B* **2012**, *85*, 115317.

[44] H. Kind, H. Yan, B. Messer, M. Law, P. Yang, *Adv. Mater.* **2002**, *14*, 158-160.

[45] T. Mueller, F. Xia, P. Avouris. *Nat. Photonics* **2010**, *4*, 297-301.

[46] O. Lopez-Sanchez, D. Lembke, M. Kayci, A. Radenovic, A. Kis, *Nat. Nanotechnol.* **2013**, *8*, 497-501.

[47] N. Youngblood, C. Chen, S. J. Koester, M. Li, *Nat. Photon*. **2015**, *9*, 247-252.

[48] D. Akinwande, N. Petrone, J. Hone. *Nat. Commun.* **2014**, *5*, 5678.

[49] G. H. Han, N. J. Kybert, C. H. Naylor, B. S. Lee, J. Ping, J. H. Park, J. Kang, S. Y. Lee, Y. H. Lee, R. Agarwal, A. T. Charlie Johnson, *Nat. Commun.* **2015**, *6*, 6128.

[50] Z. Liu, L. Ma, G. Shi, W. Zhou, Y. Gong, S. Lei, X. Yang, J. Zhang, J. Yu, K. P. Hackenberg, A. Babakhani, J.-C. Idrobo, R. Vajtai, J. Lou, P. M. Ajayan, *Nat. Nanotechnol.* **2013**, *8*, 119-124.

[51] Z. Kang, S. Xie, L. Huang, Y. Han, P. Y. Huang, K. F. Mak, C. Kim, D. Muller, J. Park, *Nature* **2015**, *520*, 656-660.

[52] H.-M. Li, D. Lee, d. Qu, X. Liu, J. Ryu, A. Seabaugh, W. J. Yoo, *Nat. Commun.* **2015**, *6*, 6564.

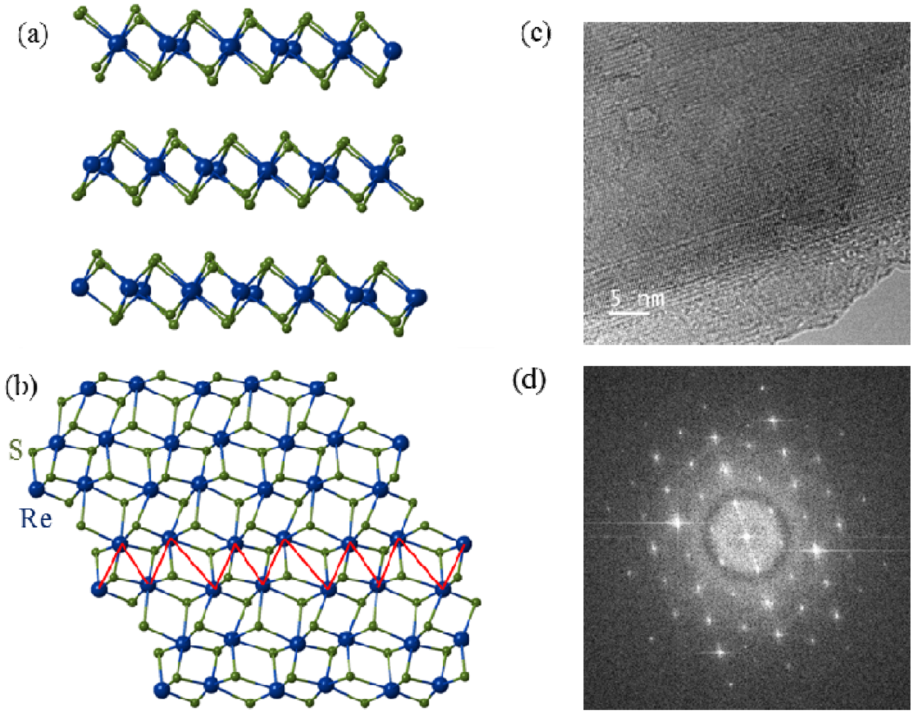

Figure 1. Crystal structure and TEM characteristics of the ReS_2. (a) Side view and (b) top view of the crystal structure. The structure shows distorted 1T structure and Re-chain along the b-axis, as indicated by the red lines. (c) The HRTEM and (d) corresponding FFT pattern of ReS_2, indicating the high crystalline of the exfoliated sample.

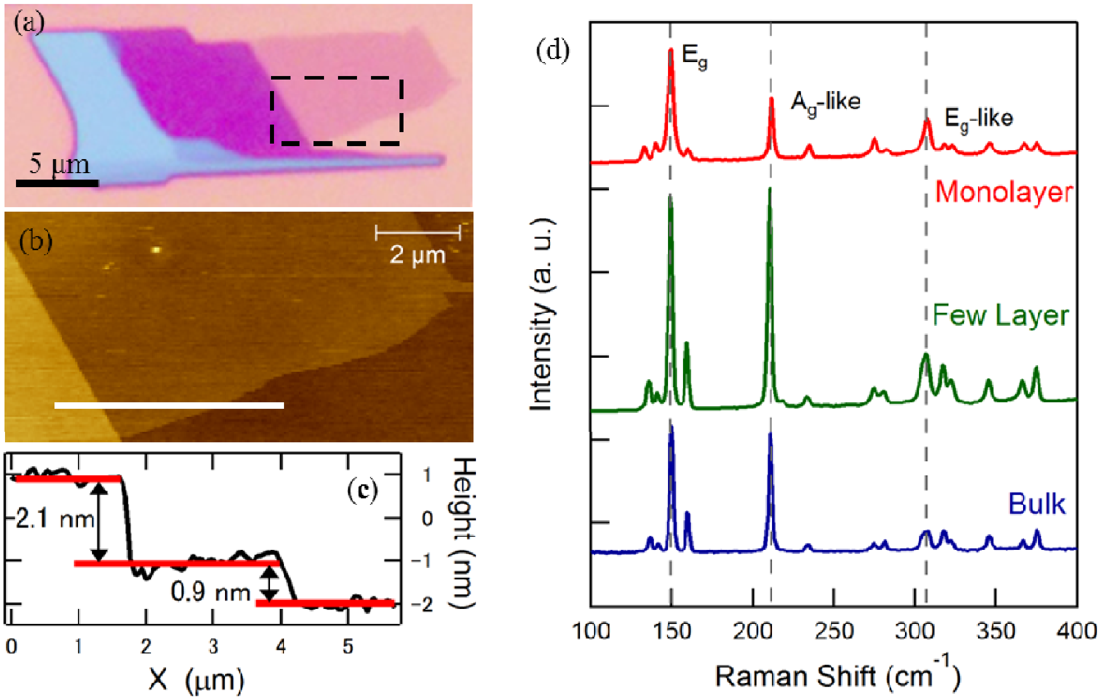

Figure 2. AFM and Raman characteristics of the ReS_2. (a) Optical image of a typical ReS_2 flake. Scale bar is 5 μm. (b) An AFM image of the area surrounded by black dashed lines in (a). (c) The line profile of the ReS_2 flake along the white line indicated in (b), showing a single-layer thickness of 0.9 nm for the monolayer range, and a thickness of 3 nm for the few layer range. (d) The Raman spectrum of bulk (blue), few layer (green) and monolayer (red) ReS_2, respectively. The main peaks at 150 cm^{-1} and 210.5 cm^{-1} are corresponding to the in-plane (E_{2g}) and mostly out-of-plane (A_{1g}-like) vibration modes, respectively. The Raman peaks are quite similar in the bulk, few-layer and monolayer forms, indicating weak interlayer coupling.

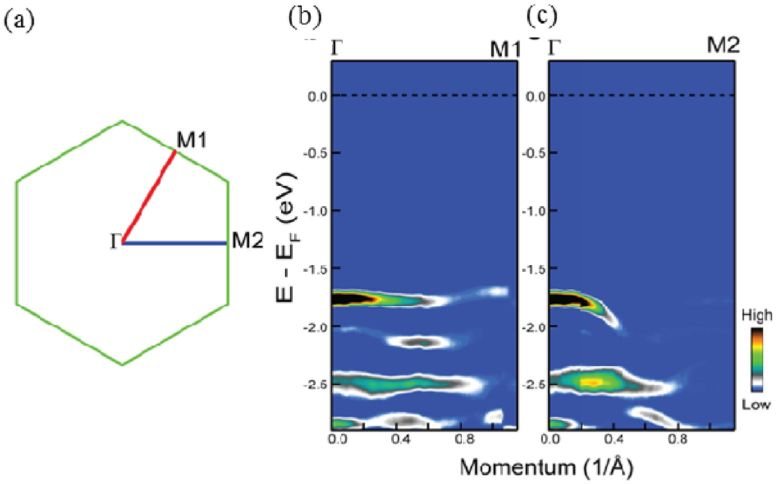

Figure 3. Anisotropic electronic structure of ReS_2. (a) Undistorted hexagonal Brillouin zone of ReS_2. The band dispersion along Γ-M1 (b) and Γ -M2 (c) with their momentum locations marked in A. The

differences between B and C indicate that the 6-fold symmetry of the hexagonal Brillouin zone is broken due to lattice distortion.

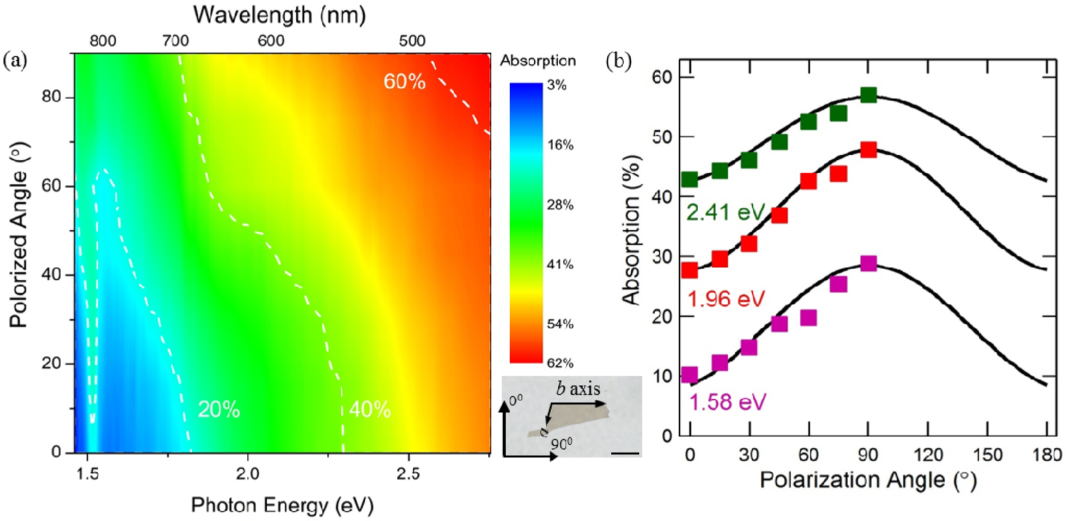

Figure 4. The polarization dependent absorption spectrum of atomically thin ReS_2. (a) Two-dimensional plot of absorption spectrum as a function of the polarization angle respect to the *b*-axis of the crystal structure. Inset of Figure a shows the optical image of the ReS_2 with a thickness of about 12 nm. The definition of angle respect to the *b* axis is also shown, which will be used in the following measurement. Scale bar, 10 μm. (b) Absorption as a function of polarization angle at different photo energies (2.41 eV, 1.96 eV and 1.58 eV, respectively). They follow the sinusoidal function fitting (black line).

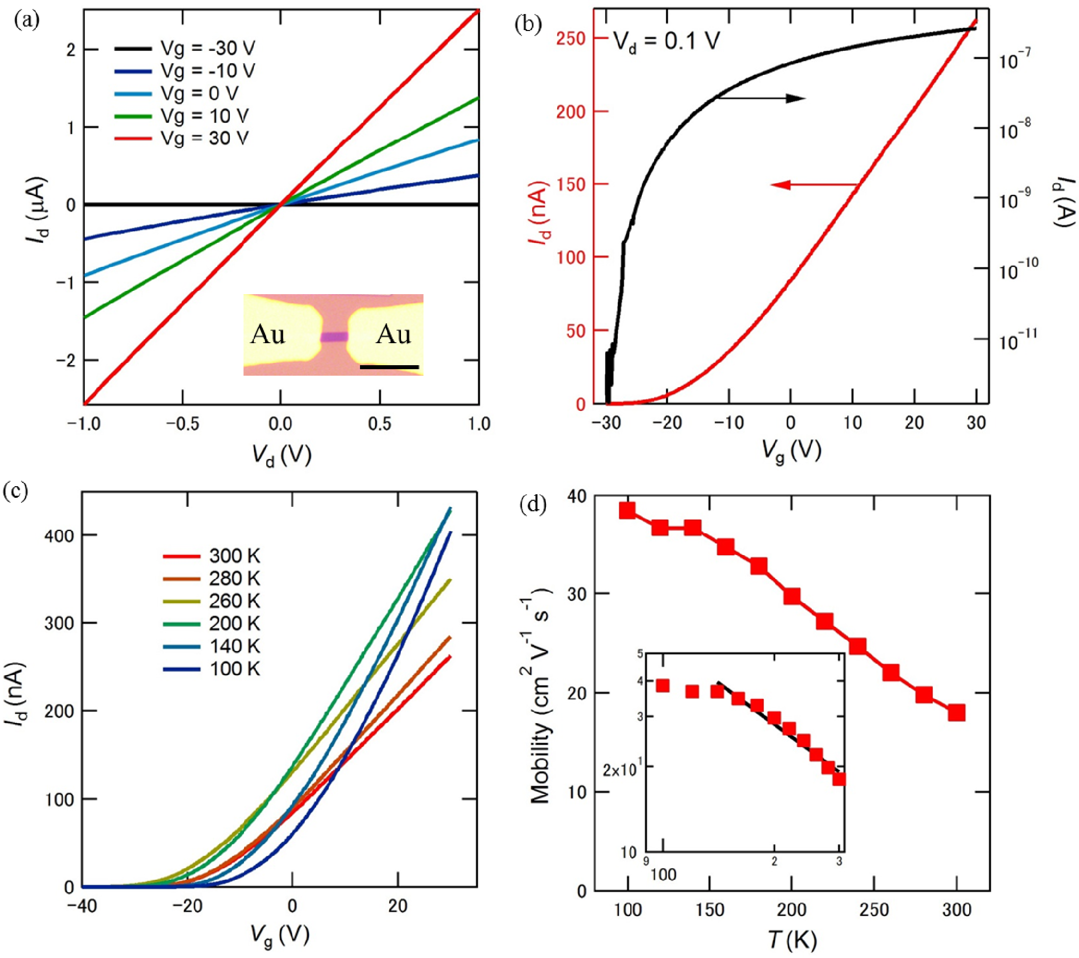

Figure 5. Characterization of the few layer ReS_2 field effect transistor. (a) Output transfer curve of the transistor at room temperature based on ReS_2 with a thickness of about 3 nm. The transistor exhibits n-type behavior and low contact resistance. The inset shows a typical optical image of the transistor. Scale bar, 10 μm. (b) The linear (red) and log (black) scale plots of the transfer curve, showing a mobility of 18 $cm^2V^{-1}s^{-1}$ with a on/off ratio of about 10^5. (c) The I_d-V_g transfer curve for the ReS_2 transistor with a drain voltage of 0.1 V acquired at different temperatures. (d) The field effect mobility as a function of temperature extracted from Figure 5c. The mobility increases gradually with decreasing temperature. The inset shows the power law fitting of the data, indicating the dominant electron-phonon scattering at higher temperature.

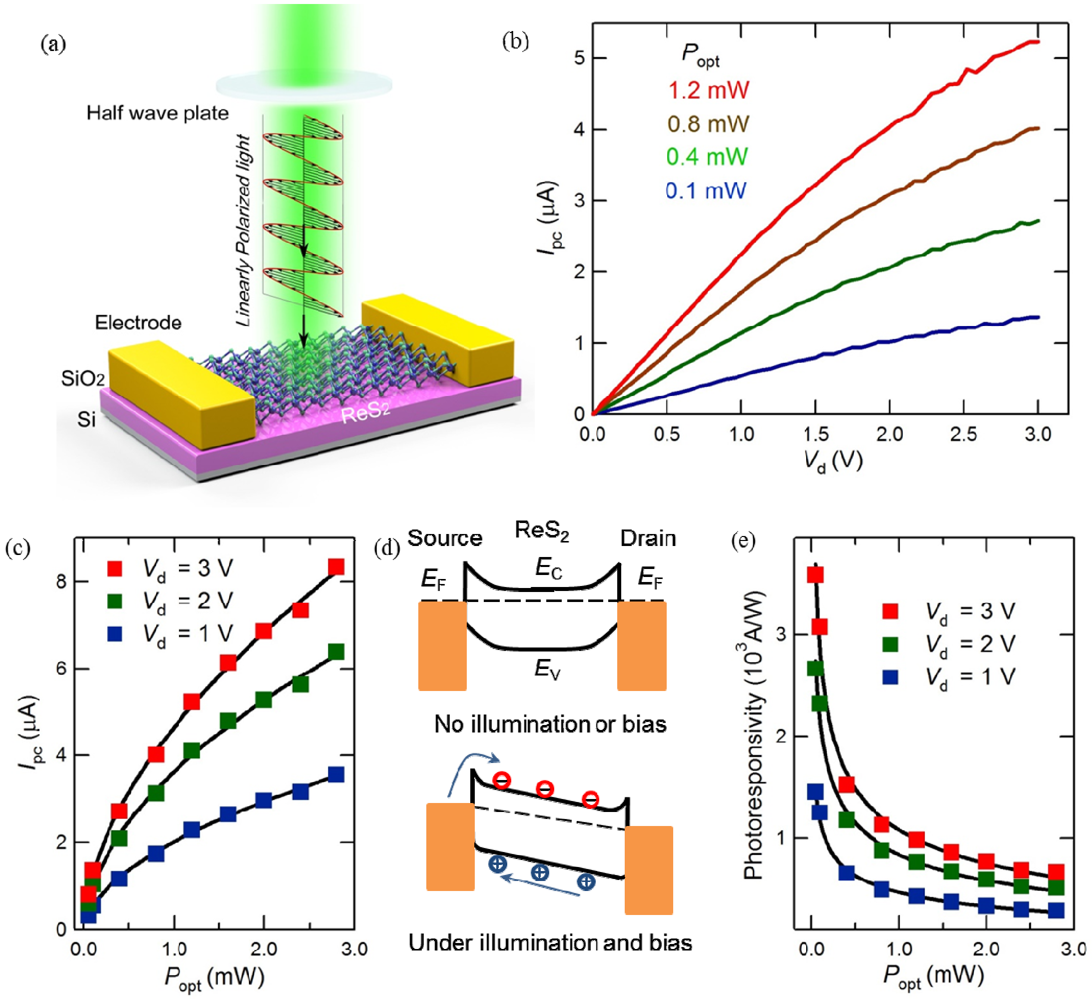

Figure 6. Photoresponse properties of the ReS_2 device. (a) Three-dimensional schematic view of the photodetection device. The light is illuminated on the ReS_2 channel, and the light polarization is controlled by the half wave plate, which is used for the linear dichroism detection later. (b) The photocurrent response as a function of drain voltage under different light intensity green light illumination. (c) the photocurrent as a function of light intensity under a drain voltage of 1 V (blue), 2 V (green) and 3 V (red), respectively. The data can be fitted very well using the power law function (black line). (d) Schematic band diagrams of the device under different illumination and bias conditions. E_F, Femi level; E_C, Conduction band; E_V, Valence band. The ReS_2 forms Schottky barriers with Cr/Au electrodes. When a light illuminates the device, electron-hole pairs are generated and separated by the applied drain voltage, generating photocurrents. (E) The light intensity dependence of photoresponsivity deduced from Figure 6c for drain voltages of 1 V (blue), 2 V (green) and 3 V (red), respectively. The black lines are guides to eyes.

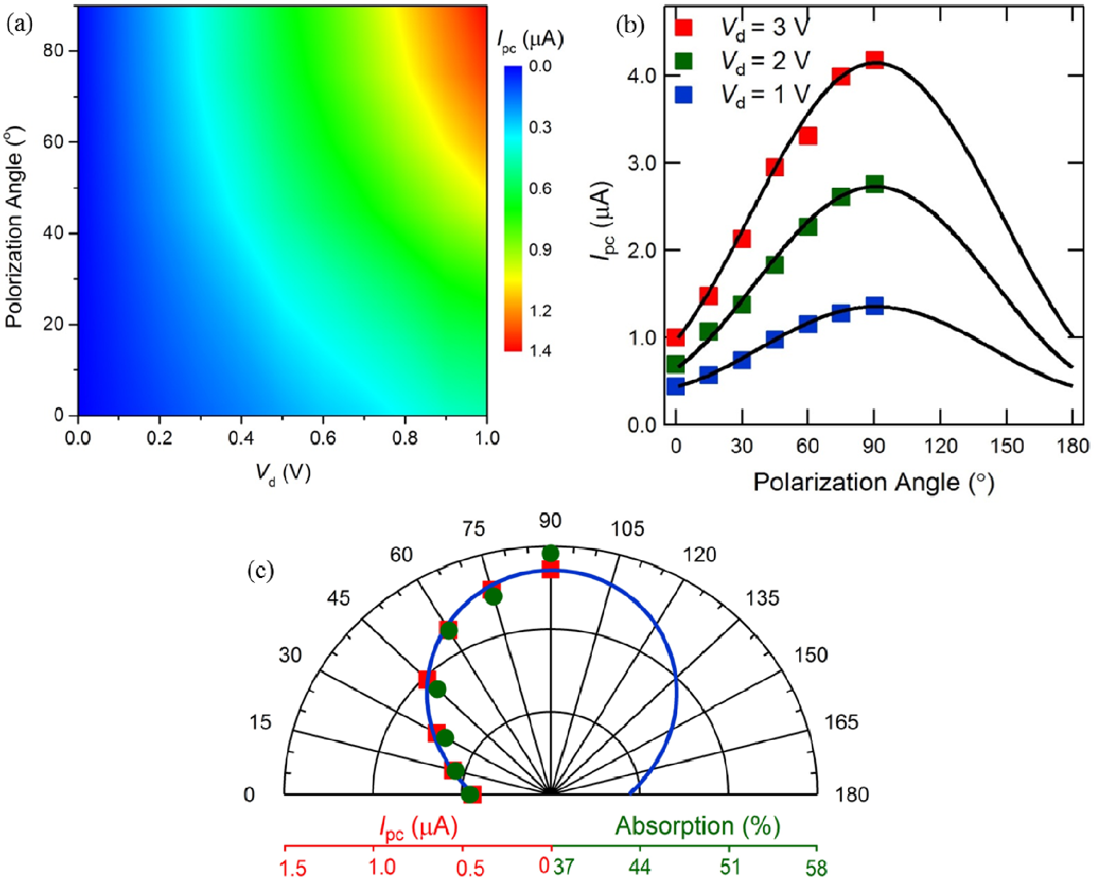

Figure 7. Polarization sensitive photoresponse of ReS_2. (a) The photocurrent change as a function of drain bias under different polarization light illuminations. (b) The change of the photocurrent under different drain biases plotted as a function of polarization angle, the data can be fitted very well using a power law function (black line). (c) The photocurrent with drain bias of 1 V (red squire) and absorption (green circle) measured under different polarization angle of green light and plotted in polar coordinates. The blue lines are the fitting results using sinusoidal function. The consistence between photocurrent and absorption indicates the intrinsic linear dichromic response of ReS_2.